Astronomy & Astrophysics manuscript no. Suhasaria_2020
July 17, 2020

Destruction route of solid-state formamide by thermal H atoms

T. Suhasaria and V. Mennella

INAF-Osservatorio Astronomico di Capodimonte, Salita Moiariello 16, 80131, Naples, Italy
e-mail: tushar.suhasaria@inaf.it

July 17, 2020

ABSTRACT

Context. Formamide (NH_2CHO) is one of the simplest "CHON" molecules that has been observed in different environments in space. In star-forming regions, its abundance in the gas phase is correlated to isocyanic acid (HNCO), indicating a chemical relation between the two species. Many studies have investigated the different routes for the transformation of the two species from one to the other.
Aims. We carry out an experimental analysis on the interaction of atomic H at 300 K with solid NH_2CHO to probe whether HNCO can form.
Methods. The effects of H atom irradiation on NH_2CHO have been analyzed by Fourier-transform infrared spectroscopy.
Results. During irradiation, a decrease in the band intensity of the C-H, C=O, and N-H modes of NH_2CHO with a simultaneous increase in the N=C=O band intensity of HNCO is observed, indicating a transformation of NH_2CHO to HNCO. The corresponding destruction and formation cross-sections have been estimated from the trend of the normalized column densities as a function of the H atom fluence. The transformation follows a three-step reaction sequence driven by H atom exothermic abstractions that also induce sputtering of the products. No bands of aminomethanol were detected.
Conclusions. The interaction of H atoms with NH_2CHO in space can be one of the promising mechanisms to explain the chemical relation between NH_2CHO and HNCO. In addition, the comparison of our results with those of other energetic processing agents suggests that H atoms play a crucial role in the destruction of NH_2CHO ice in dense regions of the interstellar medium.

Key words. astrochemistry – methods: laboratory: solid state - techniques: spectroscopic - ISM: molecules

1. Introduction

In recent years, formamide (NH_2CHO), a molecule containing an amide bond, has gained considerable interest as a promising candidate for prebiotic chemistry in space. It acts as a precursor of essential biological components of life: amino acids, nucleobases, sugars, carboxylic acids, etc. (Saladino et al. 2012; Ferus et al. 2015; Botta et al. 2018). **Formamide** was detected for the first time in space in the gas phase towards the giant molecular cloud Sgr B2 (Rubin et al. 1971). Since then, it has been observed in other astrophysical environments such as star-forming regions and comets [e.g., (Blake et al. 1986; Turner 1991; Bisschop et al. 2007; Mendoza et al. 2014; López-Sepulcre et al. 2015; Bockelée-Morvan et al. 2000; Biver et al. 2014; Goesmann et al. 2015)]. Formamide has also been tentatively identified in interstellar ices through Infrared Space Observatory spectra towards NGC 7538 IRS9 and W33A (Raunier et al. 2004; Gibb et al. 2004).

The formation mechanism of NH_2CHO is highly debated. Based on experimental and theoretical studies, it has been proposed that NH_2CHO forms in the gas phase by a series of ion-molecule and neutral-neutral reaction channels (Quan & Herbst 2007; Halfen et al. 2011; Redondo et al. 2013, 2014; Spezia et al. 2016; Garrod et al. 2008; Barone et al. 2015). On the other hand, solid NH_2CHO has been shown to form in interstellar ice analog mixtures via energetic processing, which is induced by several agents such as electrons, ions, ultraviolet (UV), vacuum-ultraviolet (VUV), and H atoms [e.g., (Bernstein et al. 1997; Muñoz Caro & Schutte 2003; Gerakines et al. 2004; Raunier et al. 2004; Jones et al. 2011; Jheeta et al. 2013; Bergantini et al. 2014; Kaňuchová et al. 2016; Urso et al. 2017; Dulieu et al. 2019)].

A specific formation route of NH_2CHO in the gas and solid phase considers isocyanic acid (HNCO) as a precursor molecule. This idea is based on astronomical observations of young stellar objects that show a tight linear correlation between HNCO and NH_2CHO abundances (López-Sepulcre et al. 2019, references therein). This result suggests that the two molecules are chemically linked and either both of them form from a common precursor or one forms from the other [e.g., (Bisschop et al. 2007; López-Sepulcre et al. 2019)].

Laboratory investigations successfully used HNCO as a starting molecule to form NH_2CHO. In a gas phase study, a mixture of HNCO and H_2 under glow discharge successfully produced NH_2CHO (Ferus et al. 2018). The result was interpreted using an ab initio molecular dynamics simulation that showed that the hydrogenation of HNCO, by both H and H_2, is the thermodynamically favored reaction pathway to NH_2CHO formation. On the other hand, in the solid phase, the VUV photodissociation of HNCO ice produces free H atoms, which react with remaining HNCO to form NH_2CHO (Raunier et al. 2004). However, no detectable amount of NH_2CHO was found in the hydrogenation experiment of HNCO that was performed at 15 K (Noble et al. 2015).

From a theoretical point of view, the hydrogenation of HNCO efficiently produces NH_2CHO in the grain mantle chemical model of Garrod et al. (2008). In addition, quantum mechanical calculations on hydrogenation of HNCO on the surface of amorphous water ice show that H atom tunneling plays an important role in the formation of NH_2CHO at low temperatures (Song & Kästner 2016).

The chemical relation between HNCO and NH_2CHO can also be explained through a reverse reaction pathway, that is, HNCO forming from NH_2CHO. In general, only a limited number of laboratory studies have been performed on the destruction of NH_2CHO under energetic processing; HNCO was not obtained in all cases. For example, under electron and Ly-α irradiation of NH_2CHO, OCN^- and CO were obtained (Dawley et al. 2014). A pure NH_2CHO ice film does not show significant degradation upon exposure to a UV-enhanced xenon lamp, whereas in the presence of oxide minerals TiO_2 and $MgAl_2O_4$, a gradual degradation was observed (Corazzi et al. 2020). Also, no reaction occurred between NH_2CHO ice and a hydrogen atom (Noble et al. 2015). On the other hand, HNCO formed along with CO_2, N_2O, CN^-, NH_4^+, OCN^-, and CO when NH_2CHO ice films were irradiated with 200 keV H^+ (Brucato et al. 2006). Very recently, HNCO also formed from NH_2CHO through **H-abstraction** reactions via a H_2NCO radical intermediate in the presence of a para-hydrogen quantum-solid matrix host (Haupa et al. 2019).

In the present work, we report the results of the interaction of thermal H atoms (300 K) with a NH_2CHO ice film at 12 K. The interaction results in the destruction of NH_2CHO and the formation of HNCO and OCN^-. The reaction sequence has been clearly identified and quantitative evaluation of NH_2CHO destruction cross-sections and a HNCO formation cross-section by H atoms have been estimated for the first time. Finally, astrophysical implications of the results are discussed.

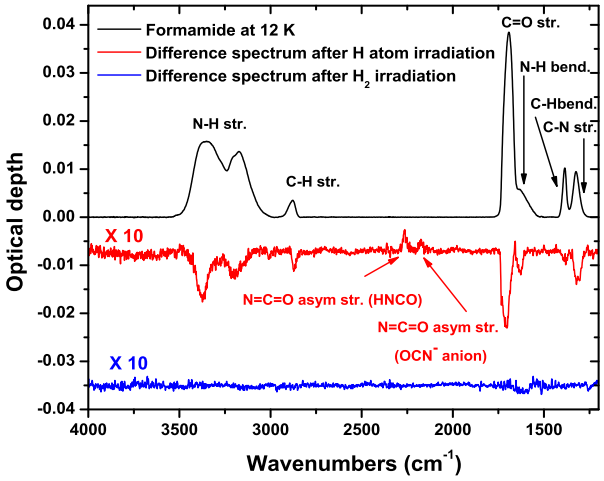

Fig. 1. IR spectrum of a 29 ML thick NH_2CHO film at 12 K (black line). The spectrum after irradiation (subtracted from the initial spectrum) of 2×10^{17} H atoms cm^{-2} (red line) is reported. The NH_2CHO spectrum after irradiation (subtracted from the initial spectrum) of 2.7×10^{17} H_2 molecules cm^{-2} (blue line) as obtained in a blank experiment is also shown for comparison purposes. The red and blue curves **are offset in ordinate by -0.007 and -0.035,** respectively, for the sake of clarity.

2. Experimental methods

The experiments were performed in a high vacuum set-up with a main chamber equipped with a closed-cycle helium cryostat (Galileo Vacuum model K1) and a dosing unit. The base pressure of the main chamber was better than 10^{-8} mbar. A CsI substrate was mounted on the cold finger of the cryostat. The substrate temperature was measured with a calibrated silicon diode mounted close to the substrate. **Formamide (EMSURE grade; Merck) liquid was purified** by several freeze-pump-thaw cycles to degas impurities and then the vapors were admitted via a precision leak valve (MDC vacuum limited) to the substrate at 12 K. The gas inlet extending from the dosing chamber (pressure $\sim10^{-6}$ mbar) was directed to the substrate inside the main chamber to ensure vapor exposure primarily to the substrate. The ice film that formed in this way is expected to result in nonhomogenous film growth as compared to a background deposition.

To irradiate the NH_2CHO ice film, an atomic hydrogen beam was produced by microwave dissociation of molecular hydrogen (99.9999% purity). The H source is made of a Pyrex tube, with a 10 mm outer diameter and 1 mm in thickness, which was inserted in an Evenson cavity operating at 2.45 GHz with 45 W microwave power. The atomic beam has a Maxwellian distribution of the velocity of H atoms at 300 K (Mennella 2006). The NH_2CHO ice film was studied in situ before and during irradiation in transmittance mode in the range 4000–700 cm^{-1} at a resolution of 2 cm^{-1} using a Fourier transform infrared (FTIR) spectrometer (Bruker Vertex 80V) with a Mercury Cadmium Telluride (MCT) detector. The substrate is at an angle of 22.5° and 67.5° with respect to the hydrogen beam and the IR beam, respectively, such that the IR spectral evolution of the sample can be monitored during irradiation. For each single measurement, 1024 scans were co-added. The background was acquired for any spectral measurement of NH_2CHO before and after each irradiation dose. The NH_2CHO ice film thickness was derived independently from the column density of N-H, C-H, and C-O stretching IR modes using the band strengths 1.35×10^{-16}, 4.7×10^{-18}, and 6.54×10^{-17} cm mol^{-1}, respectively, (Brucato et al. 2006). The average value, expressed in units of monolayer (1 ML = 10^{15} molecules cm^{-2}), is 29 ML. In determining this value, we also considered the cosine of the angle between the IR beam and the normal to the surface plane.

3. Results and discussion

Figure 1 shows the IR spectrum of a 29 ML thick NH_2CHO film deposited at 12K. The fundamental vibration modes of NH_2CHO are identified to be in agreement with previous measurements (Brucato et al. 2006; Sivaraman et al. 2013; Urso et al. 2017) and are labeled in Figure 1. A broad band is observed between 3500 and 3000 cm^{-1} with peaks centered at 3355 and 3170 cm^{-1}, respectively, which correspond to the asymmetric and symmetric stretch modes of the -NH_2 group. The band centered at 2878 cm^{-1} is assigned to the C-H stretching mode and the strongest band centered at 1690 cm^{-1} is due to the C=O stretching of the carbonyl group. The peak centered at 1631 cm^{-1} is due to the in-plane NH_2 bending (scissor) mode. This peak appears as a shoulder to the strongest band at 1690 cm^{-1}. Two additional peaks centered at 1386 and 1324 cm^{-1} are attributed to the in-plane C-H bending (scissor) and C-N stretching modes, respectively. The two peaks at around 836 and 710 cm^{-1} corresponding to the NH_2 wagging and twisting modes, respectively, could not be detected in our spectra.

Upon exposure to H atoms, the intensity of all the NH_2CHO IR bands decreases and a new band appears at 2265 cm^{-1}. Only for a fluence higher than 1.5×10^{17} H atoms cm^{-2}, a second band at 2172 cm^{-1} becomes evident. These features are assigned, respectively, to the N=C=O asymmetric stretching mode of HNCO and isocyanate anion (OCN^-) based on prior assignments (Brucato et al. 2006). It is important to note that NH_4^+ is the most likely counterion of OCN^- (see footnote 2). It has an IR fea-

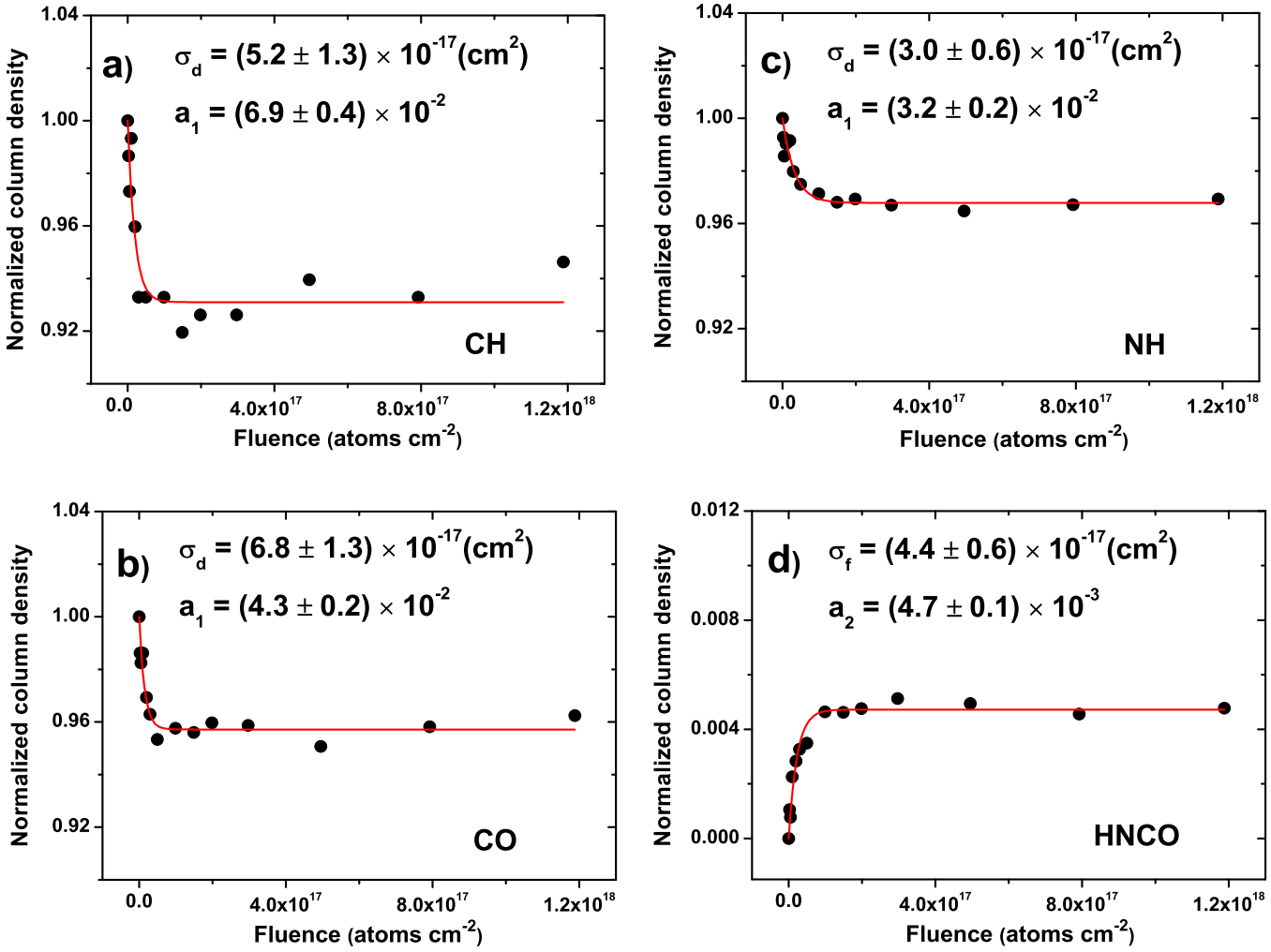

Fig. 2. Evolution with H atom fluence of the C-H (a), C=O (b), N-H (c), and N=C=O (HOCN) (d) normalized column density (filled circles). In the first three cases, the normalization factor is the corresponding initial column densities, while for HNCO, the data are normalized to the initial value of the column density of NH_2CHO. The best fit to the data (solid lines), following first order kinetic relations [$1 - a_1(1 - e^{-\sigma_d F_H})$ and $a_2(1 - e^{-\sigma_f F_H})$] are also shown. The first equation refers to the destruction with the boundary condition that considers a residual reactant for $F_H = \infty$ (i.e., H atoms cannot react with the deeper ice layers). The second equation refers to the formation limited by the availability of the reactants. The estimated destruction (σ_d) and formation (σ_f) cross-sections and the asymptotic destruction of NH_2CHO (a_1) and asymptotic formation of HNCO (a_2) are also reported.

ture at 1478 cm^{-1} (Raunier et al. 2004). We could not identify it because the expected band intensity is under the detection limit owing to a weaker band strength than OCN^- (Van Broekhuizen et al. 2004). In the difference spectrum in Figure 1, one can also see that some IR bands are slightly shifted and become sharper than the pristine NH_2CHO ice. The observed sharpening could be a sign of film crystallization. However, its amount is much less than that observed during the transition from amorphous to crystalline NH_2CHO ice (Urso et al. 2017). For instance, those authors found that the full width at half maximum (FWHM) of the C=O stretching mode decreases by 39 cm^{-1} after the transition. In contrast, after H atom exposure, we found a decrease of 7 cm^{-1} in FWHM with respect to the pristine NH_2CHO. Moreover, crystallization mostly induces a red shift of the IR bands (Sivaraman et al. 2013), whereas the peaks in our study are mainly blue shifted. Therefore, we tend to exclude crystallization and attribute the variations in the band profile to the changes in local bonding of the molecule induced by the interaction **of** H atoms.

Figure 2 shows the evolution of normalized column densities of NH_2CHO and HNCO as a function of H atom fluence, F_H. In particular, with increasing F_H, Figure 2a, 2b, and 2c show the destruction of NH_2CHO through the decrease in the intensity of C-H, C=O, and N-H stretching modes, respectively, whereas Figure 2d shows the formation of the HNCO through the increase in the intensity of the N=C=O asymmetric stretch mode. The formation of HNCO demonstrates that H atom abstraction is active. No bands due to aminomethanol at 3040 cm^{-1} (O-H stretch), 2942 cm^{-1} (CH_2 asymmetric stretch mode), and 1040 cm^{-1} (C-N+C-O stretch combination band) were present (Bossa et al. 2009). This indicates that the H atom addition to NH_2CHO is inactive.

Fits to the experimental data in Figure 2 allowed us to estimate the cross-sections and asymptotic values for the NH_2CHO destruction (σ_d, a_1) and HNCO formation (σ_f, a_2), respectively. The average of the three estimated asymptotic fit parameters $a_{1,CH}$, $a_{1,CO}$ and $a_{1,NH}$ is 4.8×10^{-2}, which corresponds to the destruction of 1.4 ML of the initial NH_2CHO ice. Destruction is thus confined to the ice surface. On the other hand, the estimated asymptotic fit parameter, a_2, for HNCO formation is 4.7×10^{-3}, corresponding to 0.14 ML. This indicates that 10% of the destroyed NH_2CHO molecules are converted into HNCO. For OCN^- observed at the highest fluences, the average values for the column density[1], which are normalized with respect to the initial NH_2CHO ice thickness (29 ML), are around 1.4×10^{-3}, corresponding to 0.04 ML. This means that ∼3% of the destroyed NH_2CHO molecules result in the formation of OCN^-.

The estimated destruction cross-section of $\sigma_{d,CH}$ and $\sigma_{d,CO}$ are equal within the error and are larger than $\sigma_{d,NH}$ suggesting that a H atom interaction induces the transformation of NH_2CHO to HNCO through the following reaction sequence:

1. H abstraction from the C-H group:

$$H + NH_2CHO \rightarrow NH_2CO + H_{2,gas}; \quad (1)$$

2. Rearrangement around the carbonyl group;
3. H abstraction from the -NH_2 group:

$$H + NH_2CO \rightarrow HNCO + H_{2,gas}. \quad (2)$$

The similarity of the $\sigma_{d,NH}$ and $\sigma_{f,NCO}$ cross-sections suggests that H atom abstraction from the -NH_2 group is the rate-limiting step for both NH_2CHO destruction and HNCO formation. Our results are in agreement with the recent findings by Haupa et al. (2019), who studied the interaction of H atoms with NH_2CHO in a para-hydrogen quantum-solid matrix at 3.3 K. These authors observed the formation of HNCO via NH_2CO intermediate through Reactions [(1) and (2)]. Furthermore, potential energy computations revealed that the first H atom abstraction from the C-H group of NH_2CHO [Reaction (1)] has an activation barrier of 0.27 eV (3130 K), while the second H atom abstraction from the NH_2CO [Reaction (2)] is barrierless[2]. In our study, the energy of thermal H atoms (300 K) is also well below the activation barrier. Therefore, similar to the findings of Haupa et al. (2019), the first H atom abstraction proceeds through quantum tunneling.

We have found two interesting results regarding the interaction of H atoms with NH_2CHO ice: the low reaction yield and the destruction of a limited fraction of the initial NH_2CHO molecules (see the saturation of the normalized column densities at an average ∼95% in Figure 2). Concerning the low reaction yield, we have estimated that only ∼13% of the destroyed NH_2CHO molecules are converted into HNCO and OCN^-. No other reaction products have been identified by infrared spectroscopy. We exclude the sputtering of NH_2CHO molecules due to the energy of 300 K H atoms as the cause of the low yield. In fact, we did not find any spectral variation in a blank experiment (see Figure 1) by exposing NH_2CHO ice to H_2 molecules. In that experiment, we have a similar interaction energy as for H atoms but without their reactivity. Alternatively, the low yield could be due to the sputtering of reactants and/or products induced by the reaction of H atoms with NH_2CHO ice. In the sequence described above, the two H atom abstractions, forming NH_2CO, HNCO, and two H_2 molecules, are exothermic (Haupa et al. 2019). In general, the H atom recombination to H_2 releases 4.5 eV of energy. For H_2 formation in chemisorbed sites, the exoenergeticity is reduced due to the bond breaking: C-H in [Reaction (1)] and N-H in [Reaction (2)]). From the potential energy diagram calculations reported by Haupa et al. (2019), one can deduce a net energy release of ∼0.5 eV in Reaction (1) and ∼3.3 eV in Reaction (2). This energy goes into the kinetic energy and internal excitation energy of the newly formed H_2 molecules. In addition, a fraction of the energy goes to molecules that remained in the ice after H atom abstractions. Energy partitioning is not well defined, so equipartition among the three possibilities is commonly assumed [e.g., (Black & Dalgarno 1976; Shaw et al. 2005)]. This means ∼1/3 fraction of the net available energy, that is to say, 0.17 eV [in Reaction (1)] and 1.1 eV [in Reaction (2)] goes primarily to NH_2CO and HNCO molecules, respectively. Since most of the energy is received by HNCO and as its binding energy[3] is the lowest among the three considered molecules, we expect its selective sputtering to be the reason for the observed low yield with respect to the NH_2CHO that was destroyed by the interaction of H atoms. In situ mass spectroscopic measurements could be useful to confirm this interpretation from an experimental point of view by detecting HNCO that was released in the gas phase during the interaction of H atoms with NH_2CHO. Furthermore, a H atom recombination occurring on NH_2CHO could also contribute to the nonselective sputtering of all the species present in the ice. In fact, in this case, 1.5 eV of the energy is released to the ice surface and it exceeds the binding energies of all the species.

On the other hand, concerning the destruction of a limited fraction of the initial NH_2CHO, we have identified some factors that could determine this result. First, the interaction takes place on the ice surface as H atoms (with little meV energy) cannot penetrate the entire ice layer. Second, we have to consider that the addition of H atoms to HNCO, forming NH_2CHO, is active (Haupa et al. 2019). Therefore, the total destruction of NH_2CHO molecules reacting with H atoms is not anticipated, rather an equilibrium value of their number is expected as determined by the efficiency of the two competitive processes (i.e., addition and abstraction of H atoms). Finally, the sputtering of molecules, as discussed above, has to be also taken into account.

In the end, we want to stress that the estimated destruction cross-section of NH_2CHO and the formation cross-section of HNCO are a good representative of all the involved processes –abstraction, sputtering, and addition – during the interaction of H atoms with NH_2CHO ice. The estimated cross-sections should then be considered as effective quantities rather than being referred to as a single process. Our results thus extend the possibility of NH_2CHO ice destruction via H atom abstraction to experimental conditions which are more similar to dense cloud conditions **than those met in laboratory experiments that have been performed so far.**

[1] Calculated assuming band strength of 1.3×10^{-16} cm mol^{-1} (Van Broekhuizen et al. 2004).

[2] The H atom addition to NH_2CO forming NH_2CHO is also barrierless (Haupa et al. 2019). The formed NH_2CO radical can also react with H atoms producing NH_3 and CO (Woolley & Back 1968). Isocyanic acid will react with NH_3 to form NH_4^+ OCN^-.

[3] The binding energies of NH_2CHO, NH_2CO, and HNCO are 0.7, 0.5, and 0.3 eV, respectively (Noble et al. 2015; Penteado et al. 2017; Chaabouni et al. 2018).

4. Astrophysical implications

In space, NH_2CHO is exposed to various agents such as UV photons, cosmic rays, electrons, and atom bombardment (mainly H), which can lead to its destruction and, at the same time, lead to the formation of new species. Laboratory measurements, under simulated space conditions, of destruction and formation cross-section of NH_2CHO are, therefore, essential to understanding its stability and evolution in interstellar space. In fact, these quantities are typically used in physico-chemical models to determine molecular abundances.

Isocyanic acid formed due to the **interaction of 300 K H atoms with NH_2CHO**. The H atom abstractions sequence from NH_2CHO ice confirms the findings by Haupa et al. (2019) and points to a promising mechanism to interpret the tight linear correlation of the molecular abundances of these two species in star forming regions. In addition, the knowledge of the destruction cross-section of NH_2CHO by H atoms allows us to estimate the contribution of this reaction channel with respect to other destructive mechanisms that are active in space. In fact, using the destruction cross-section, σ_d, the corresponding destruction rate of a molecule in a specific environment, $R_d = \sigma_d \Phi$, can be estimated knowing the flux, Φ, of the acting agent in space. In the case of H atoms, we estimated a conservative value for R_d using $\sigma_{d,H}$ (i.e., $\sigma_{d,NH}$) $= 3.0 \pm 0.6 \times 10^{-17}$ cm^2, which was obtained for the rate-limiting step of NH_2CHO destruction. However, one can also use $\sigma_{d,CH}$ since NH_2CHO molecules are already destroyed after the first H atom abstraction. Moreover, the NH_2CHO destruction cross-section obtained in the present work is more relevant to evaluating the destruction rate for dense cloud conditions and the derived rates for diffuse conditions are meant for comparison purposes only. We adopted the hydrogen flux $\Phi_H = 8 \times 10^6$ H atoms cm^{-2} s^{-1} (Sorrell 1990) and $\Phi_H = 9.1 \times 10^4$ H atoms cm^{-2} s^{-1} (Mennella 2006) for diffuse and dense regions of the insterstellar medium (ISM), respectively. The derived rates are $R_{d,H,diffuse} = 2.4 \times 10^{-10}$ s^{-1} and $R_{d,H,dense} = 2.7 \times 10^{-12}$ s^{-1}. The fluxes and destruction rates are reported in Table 1.

In order to compare the effects in space of other processing agents on NH_2CHO, there is the need to evaluate the destruction rates in a similar way as was done for H atoms. **The destruction cross-section of the NH_2CHO ice film at 17 K by 200 keV H^+ ions was recently estimated** from the intensity decrease in the C-H bending and C-N stretching modes in NH_2CHO as a function of ion fluence (G. A. Baratta & M. E. Palumbo, 2020, priv. comm.). The destructive effects of cosmic ray irradiation on NH_2CHO can, therefore, be estimated. With this aim, we applied the approximation of monoenergetic 1 MeV protons and adopted the effective flux of 1 MeV protons in diffuse, $\Phi_{1MeV} = 1.8$ protons cm^{-2} s^{-1} and dense, $\Phi_{1MeV} = 1$ protons cm^{-2} s^{-1} regions, respectively (Mennella et al. 2003, references therein). The destruction cross-section for 1 MeV protons, $\sigma_{d,1MeV} = 3.7 \pm 0.4 \times 10^{-16}$ cm^2, was obtained from the one derived from the experiment with 200 keV protons, taking the difference in the stopping power of protons at those two energies into account (G. A. Baratta & M. E. Palumbo, 2020, priv. comm.). The corresponding rates are $R_{d,1MeV,diffuse} = 6.7 \times 10^{-16}$ s^{-1} and $R_{d,1MeV,dense} = 3.7 \times 10^{-16}$ s^{-1} (see also Table 1). We note that although $\sigma_{d,1MeV} \sim 10\ \sigma_{d,H}$, the high H atom flux in both the diffuse and dense medium determines a destruction rate by at least four orders of magnitude higher than the one by cosmic rays. Therefore, we can conclude that the H atom has a more profound influence on NH_2CHO destruction in the diffuse and dense ISM as compared to the effect by cosmic rays.

Very recently, Corazzi et al. (2020) performed a laboratory experiment on UV photoprocessing of pure NH_2CHO ice. They did not find a significant degradation of NH_2CHO, consequently the destruction cross-section could not be evaluated. On the other hand, in the presence of oxide and silicate minerals, a gradual degradation of NH_2CHO was observed and a destruction cross-section in the range of 10^{-19}–10^{-20} cm^2 was derived. We note that these values are two to three orders of magnitude lower than what was obtained by H atom irradiation. In that work, a UV-enhanced xenon lamp was used as a source to resemble the effect of the radiation of solar-type stars on the NH_2CHO molecule. The energy of photons from the source is lower than atomic and molecular hydrogen UV emission, which is predominant in the diffuse and dense regions of the ISM. We cannot use those destruction cross-sections by UV photons to estimate the corresponding destruction rate in space as was done for H atoms and cosmic rays. Nonetheless, some considerations as to the effects of UV photons are still possible. Let us assume that UV irradiation of NH_2CHO gives rise to the same destruction rate as that obtained for H atoms. As an example, in dense regions we would have $R_{d,UV} = R_{d,H} = 3.6 \times 10^{-12}$ s^{-1}. Adopting the UV flux, $\Phi_{UV} = 4.8 \times 10^3$ photons cm^{-2} s^{-1} for these regions (see Table 1), we obtained the destruction cross-section, $\sigma_{d,UV} = 7.5 \times 10^{-16}$ cm^2. This value is unrealistically high since it is comparable to what was estimated for 1 MeV protons. Unlike high energy protons, which induce multiple bond breaking along the **"hot track"** when they interact with a solid, 10 eV UV photons typically induce a single photolysis event. Therefore, the UV destruction cross-section should be lower than that of the 1 MeV protons. In fact, in the case of hydrogenated carbon grains, the destruction cross-section of C-H bonds by UV photons is four orders of magnitude lower than that by the 1 MeV protons (Mennella et al. 2003). Our assumption that $R_{d,UV} = R_{d,H}$ does not hold; $R_{d,UV}$ should be significantly lower for H atoms. This conclusion should be verified by a dedicated experiment on Ly-α photoprocessing of NH_2CHO. However, it is clear that the interaction of H atoms with NH_2CHO is the driving mechanism for its destruction in the regions of the ISM.

5. Conclusions

The interaction of 300 K H atoms with NH_2CHO ice at 12 K has been studied under high vacuum conditions to simulate the reactions in interstellar space. Infrared spectroscopy has been used to analyze the results. The main conclusions derived from this work are as follows.

– An interaction results in the destruction of NH_2CHO, forming HNCO and OCN^-.

– The destruction of NH_2CHO to HNCO occurs in three steps: the abstraction of a H atom from C-H, the rearrangement around C=O, and the H abstraction from N-H bonds. In addition, the energy released during the interaction can induce sputtering of the products.

– For the first time, the effective destruction cross-section of NH_2CHO and the effective formation cross-section of HNCO, due to H atom interaction with NH_2CHO ice, are estimated.

– **In dense regions of ISM, the destruction rate of NH_2CHO by H atoms is four orders of magnitude higher than that obtained for cosmic rays.**

H atoms thus play a decisive role in the chemistry of NH_2CHO ice in dense regions of the ISM.

Acknowledgements. This work has been supported by the project PRIN-INAF 2016 "The Cradle of Life- GENESIS- SKA" (General Conditions in Early Planetary Systems for the rise of life with SKA).

Table 1. Destruction cross-sections of NH_2CHO and the corresponding rates in the ISM.

Processing	Destruction cross-section σ_d, (cm^2)	Flux Φ, (cm^{-2} s^{-1})		Destruction rate R_d, (s^{-1})	
		Diffuse	Dense	Diffuse	Dense
H atoms	$3.0 \pm 0.6 \times 10^{-17}$	8×10^6	9.1×10^4	2.4×10^{-10}	2.7×10^{-12}
Cosmic rays[a]	$3.7 \pm 0.4 \times 10^{-16}$	1.8	1	6.7×10^{-16}	3.7×10^{-16}
UV photons[b]	10^{-19}– 10^{-20}[c]	8×10^7[d]	4.8×10^3[e]		

Notes. [(a)] corresponds to 1 MeV protons under monoenergetic approximation (G. A. Baratta & M. E. Palumbo, 2020, priv. comm.)
[(b)] photons from UV-enhanced xenon lamp
[(c)] cross-section of NH_2CHO deposited on oxides and minerals (Corazzi et al. 2020)
[(d)] corresponds to 10 eV photons (Mathis et al. 1983)
[(e)] corresponds to 10 eV photons (Mennella et al. 2003)

References

Barone, V., Latouche, C., Skouteris, D., et al. 2015, MNRASL, 453, L31
Bergantini, A., Pilling, S., Nair, B., Mason, N., & Fraser, H. 2014, A & A, 570, A120
Bernstein, M., Allamandola, L., & Sandford, S. 1997, Adv. Space Res., 19, 991
Bisschop, S. E., Jørgensen, J., Van Dishoeck, E., & De Wachter, E. 2007, A & A, 465, 913
Biver, N., Bockelée-Morvan, D., Debout, V., et al. 2014, A & A, 566, L5
Black, J. H. & Dalgarno, A. 1976, ApJ, 203, 132
Blake, G. A., Sutton, E., Masson, C., & Phillips, T. 1986, ApJS, 60, 357
Bockelée-Morvan, D., Lis, D., Wink, J., et al. 2000, A & A, 353, 1101
Bossa, J. B., Theule, P., Duvernay, F., & Chiavassa, T. 2009, ApJ, 707, 1524
Botta, L., Saladino, R., Bizzarri, B. M., et al. 2018, Adv. Space Res., 62, 2372
Brucato, J. R., Baratta, G. A., & Strazzulla, G. 2006, A & A, 455, 395
Chaabouni, H., Diana, S., Nguyen, T., & Dulieu, F. 2018, A & A, 612, A47
Corazzi, M. A., Fedele, D., Poggiali, G., & Brucato, J. R. 2020, A & A, 636, A63
Dawley, M. M., Pirim, C., & Orlando, T. M. 2014, J. Phys. Chem. A, 118, 1228
Dulieu, F., Nguyen, T., Congiu, E., Baouche, S., & Taquet, V. 2019, MNRASL, 484, L119
Ferus, M., Laitl, V., Knizek, A., et al. 2018, A & A, 616, A150
Ferus, M., Nesvorný, D., Šponer, J., et al. 2015, Proc. Natl. Acad. Sci., 112, 657
Garrod, R. T., Weaver, S. L. W., & Herbst, E. 2008, ApJ, 682, 283
Gerakines, P., Moore, M., & Hudson, R. 2004, Icarus, 170, 202
Gibb, E., Whittet, D., Boogert, A., & Tielens, A. 2004, ApJS, 151, 35
Goesmann, F., Rosenbauer, H., Bredehöft, J. H., et al. 2015, Science, 349
Halfen, D., Ilyushin, V., & Ziurys, L. M. 2011, ApJ, 743, 60
Haupa, K. A., Tarczay, G., & Lee, Y.-P. 2019, J. Am. Chem. Soc., 141, 11614
Jheeta, S., Domaracka, A., Ptasinska, S., Sivaraman, B., & Mason, N. 2013, Chem. Phys. Lett., 556, 359
Jones, B. M., Bennett, C. J., & Kaiser, R. I. 2011, ApJ, 734, 78
Kaňuchová, Z., Urso, R., Baratta, G., et al. 2016, A & A, 585, A155
López-Sepulcre, A., Balucani, N., Ceccarelli, C., et al. 2019, ACS Earth Space Chem., 3, 2122
López-Sepulcre, A., Jaber, A. A., Mendoza, E., et al. 2015, MNRAS, 449, 2438
Mathis, J. S., Mezger, P. G., & Panagia, N. 1983, A & A, 128, 212
Mendoza, E., Lefloch, B., López-Sepulcre, A., et al. 2014, MNRAS, 445, 151
Mennella, V. 2006, ApJL, 647, L49
Mennella, V., Baratta, G., Esposito, A., Ferini, G., & Pendleton, Y. 2003, ApJ, 587, 727
Muñoz Caro, G. M. & Schutte, W. A. 2003, A & A, 412, 121
Noble, J., Theule, P., Congiu, E., et al. 2015, A & A, 576, A91
Penteado, E. M., Walsh, C., & Cuppen, H. M. 2017, ApJ, 844, 71
Quan, D. & Herbst, E. 2007, A & A, 474, 521
Raunier, S., Chiavassa, T., Duvernay, F., et al. 2004, A & A, 416, 165
Redondo, P., Barrientos, C., & Largo, A. 2013, ApJ, 780, 181
Redondo, P., Barrientos, C., & Largo, A. 2014, ApJ, 793, 32
Rubin, R. H., Swenson, G. W., J., Benson, R. C., Tigelaar, H. L., & Flygare, W. H. 1971, ApJ, 169, L39
Saladino, R., Crestini, C., Pino, S., Costanzo, G., & Mauro, E. D. 2012, Phys. Life Rev., 9, 84
Shaw, G., Ferland, G. J., Abel, N. P., Stancil, P. C., & Van Hoof, P. 2005, ApJ, 624, 794
Sivaraman, B., Sekhar, B. R., Nair, B., Hatode, V., & Mason, N. 2013, Spectrochim. Acta A, 105, 238
Song, L. & Kästner, J. 2016, Phys. Chem. Chem. Phys., 18, 29278
Sorrell, W. H. 1990, ApJ, 361, 150
Spezia, R., Jeanvoine, Y., Hase, W. L., Song, K., & Largo, A. 2016, ApJ, 826, 107
Turner, B. 1991, ApJS, 76, 617
Urso, R. G., Scirè, C., Baratta, G. A., et al. 2017, Phys. Chem. Chem. Phys., 19, 21759
Van Broekhuizen, F. A., Keane, J. V., & Schutte, W. A. 2004, A & A, 415, 425
Woolley, W. D. & Back, R. A. 1968, Canadian Journal of Chemistry, 46, 295